Available online at www.sciencedirect.com
ScienceDirect
International Journal of Fatigue 29 (2007) 1402–1412
International Journal of Fatigue
www.elsevier.com/locate/ijfatigue

Fatigue performance of sandwich beams with a pyramidal core

F. Côté, N.A. Fleck, V.S. Deshpande *

Cambridge University Engineering Department, Trumpington Street, Cambridge CB2 1PZ, UK

Received 18 May 2006; received in revised form 7 November 2006; accepted 15 November 2006
Available online 22 January 2007

Abstract

Sandwich beams have been manufactured from AISI type 304 stainless steel faces and AL6XN pyramidal core, and subjected to both monotonic and cyclic three-point bending in order to assess their monotonic and cyclic strengths. Collapse mechanisms maps for monotonic loading, and fatigue maps for cyclic loading are constructed with the aid of simple analytical models for the competing failure modes. These maps serve as useful design guides, and take the sandwich beam geometry as axes. The construction of the maps takes as input independent measured values for the monotonic and cyclic strengths of the faces and of the pyramidal core. Good agreement is found between the predicted and observed failure modes and strengths for both the static and fatigue tests. In particular, *S–N* fatigue curves for core shear are obtained from single-lap shear tests and from three-point bending tests, and are in close agreement.

Keywords: Pyramidal core; Fatigue; Shear strength; Sandwich panels

1. Introduction

Cellular materials possess combinations of mechanical properties that make them attractive in sandwich-core construction for multifunctional applications [1]. They can be classified as either stochastic foams, such as aluminium alloy foams or as micro-architectured lattice materials, such as the hexagonal honeycomb. It is now appreciated that it is the degree of nodal connectivity of an open-celled porous solid that dictates its mechanical properties more than the degree of randomness of microstructure. Superior mechanical properties can be achieved by lattice materials of high nodal connectivity, for example the octet–truss microstructure with a bar–bar connectivity of 12 per joint [2], metallic foams with a connectivity 3–4. There now exists a wide range of possible sandwich core topology, cell size and relative density in order to achieve the optimal combination of material properties: stiffness and strength (both compressive and shear), level of energy absorption, vibration and acoustic damping as well as electrical and thermal conductivity [3,4]. Relating these properties to core topology has been the focus of much recent research (see for example [5]).

Sandwich structures are commonly subjected to cyclic in-service loading, and consequently, their fatigue performance is of concern. Little is known about the fatigue response of periodic lattice materials, and our current understanding is guided by the existing literature on the fatigue properties of metallic foams. Harte et al. [6] measured the cyclic tension–tension and compression–compression properties of closed cell Alporas and open cell Duocel aluminium foams. Similarly, Sugimura et al. [7] measured the fatigue characteristics of Alporas foam under compression–compression loading. In both studies, *S–N* tests were performed, with the ratio R of minimum stress $|\sigma_{\min}|$ to maximum stress $|\sigma_{\max}|$ held constant at 0.1 and 0.5. The failure mechanisms of these foams are by cyclic ratcheting of the cell walls under tension–tension loading, and by the progressive development of crush bands in compression–compression fatigue. The endurance limit (at 10^7 cycles) for both tension–tension loading and compression–compression loading was found to be $|\sigma_{\max}| = 0.65\sigma_{\text{pl}}$ for $R = 0.1$, where σ_{pl} is the plateau strength of the foam

* Corresponding author. Fax: +44 1223 332662.
E-mail address: vsd@eng.cam.ac.uk (V.S. Deshpande).

0142-1123/$ - see front matter © 2006 Elsevier Ltd. All rights reserved.
doi:10.1016/j.ijfatigue.2006.11.013

under monotonic compression. This value is comparable to that observed for tension–tension loading of fully dense aluminium alloys [8]. In a related study, McCullough et al. [9] found that material ratcheting was the dominant cyclic deformation mode of closed cell Alulight foam in both tension–tension and compression–compression loading. They developed a simple analytical model for the prediction of fatigue life by modifying the creep model of Gibson and Ashby [1].

Sandwich cores are designed to carry predominantly shear loads, and so it is important to measure the cyclic shear response of candidate cores. Harte et al. [10] employed a cyclic double-lap shear test in order to measure the fatigue strength of Alporas foam at $R = 0.1$. Failure was by the development of distributed tensile microcracks, and they found that the normalised fatigue limit is $\tau_{max}/\tau_p \approx 0.35$, where τ_p is the peak monotonic strength. We note that the knock-down in fatigue strength is much larger for shear loading than for tension–tension loading and for compression–compression loading. Similar knock-down factors in shear fatigue have been measured for PVC foams [11], aluminium honeycombs [12] and Nomex honeycombs [13].

It is envisaged that the collapse modes for cyclic loading of sandwich beams with a periodic lattice core are similar to those under monotonic loading. Harte et al. [10] have made a similar argument for sandwich beams with a metallic foam core: the static collapse modes of core shear, face-sheet indentation and face-sheet yield are modified by cyclic loading to core fatigue, indentation fatigue and face-sheet tensile fatigue. For the case of sandwich beams with a periodic lattice core, the competing monotonic collapse modes include core shear, face-sheet indentation, face-sheet yield and face-sheet wrinkling, see for example [14]. It is envisaged that fatigue versions of these collapse modes become active under cyclic loading, with an attendant knockdown in strength compared to the monotonic collapse loads.

The intense research activity over the last few years in lattice materials has concentrated on their monotonic quasi-static and dynamic properties. Little or no data exist on their fatigue properties and this study aims address this deficiency. In particular we investigate the fatigue properties of AL6XN stainless steel pyramidal cores (Fig. 1) and then evaluate the fatigue behaviour of sandwich beams comprising AISI 304 stainless steel face-sheets and the pyramidal lattice cores. The organisation of the paper is as follows. First, the monotonic and fatigue properties of the face-sheet and core materials are measured. Second, limit load analytical methods are used to predict the collapse strength of the sandwich beams in three-point bending, taking the measured constituent strengths as input. The accuracy of the map is checked by measuring the collapse response (and observing the dominant collapse mechanisms) for a set of beams. Third, a failure mechanism map is generated for cyclic loading, by suitably modifying the limit load analyses, and by taking as input the measured *S–N* fatigue curves for the faces and core. Finally, the fatigue map is validated by performing cyclic bend tests on selected geometries.

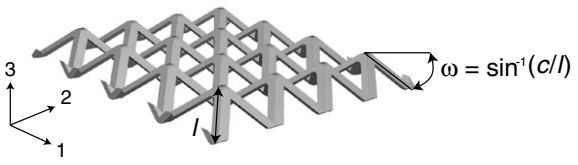

Fig. 1. Isometric view of a rectangular base pyramidal truss core with rectangular cross-section struts.

2. Monotonic and cyclic strength of the constituents

2.1. Manufacture of AL6XN stainless steel pyramidal core

AL6XN stainless steel pyramidal cores, as shown in Fig. 1, have been manufactured by perforating square holes in 0.85 mm thick sheet. The perforated sheet was folded in a concertina-like fashion to generate a pyramidal truss core with struts of rectangular cross-section [15]. The struts are of length $l = 11.5$ mm, rectangular cross-section (of dimension $t_1 = 0.85$ mm by $t_2 = 1.90$ mm), and inclination $\omega = 38.4°$, as sketched in Figs 1 and 2. The core has a relative density that can be estimated as

$$\bar{\rho} = \frac{2}{\cos^2\omega \sin\omega}\frac{t_1 t_2}{l^2} = 0.066. \quad (1)$$

In order to measure the static and fatigue strength of this pyramidal core in sandwich configuration, it is necessary to first bond the core to suitable face-sheets. We chose to bond the core to the same face sheet material as that used in the sandwich beam study reported below: the core was brazed to 25 mm thick AISI 304 stainless steel sheet, using a Ni–Cr 25-P10 (wt.%) braze. First, the core and faces were

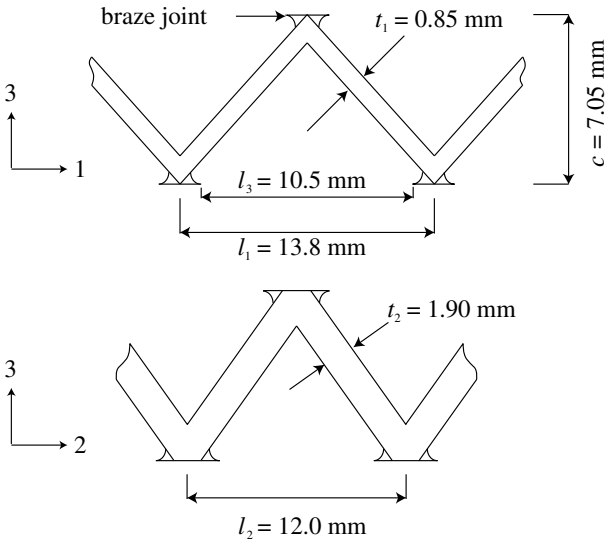

Fig. 2. Dimensions of the pyramidal core used in the present study.

uniformly coated with the brazing slurry, and were then bonded together for 1 h in a vacuum furnace at 1075 °C, using a dry argon atmosphere at 3–10 Pa. Since the folding process introduced irregularities in flatness, additional braze material was used to form the junctions between face-sheet and pyramidal core, as sketched in Fig. 2.

2.2. Monotonic out-of-plane compressive response, and out-of-plane shear response of the AL6XN pyramidal core

The out-of-plane compressive response (i.e. σ_{33} versus ε_{33}) of the pyramidal core was measured for the pyramidal core in sandwich configuration. Compression tests were performed in a screw-driven test machine using at a strain rate of $10^{-4}\,s^{-1}$ (average rate upon treating the core as a continuum). The specimens contained three cells in the length direction (x_1), and three cells in the width direction (x_2), and linear bearings were placed between the platens and the face-sheets of the specimens in order to minimize shear loading. The applied normal load was measured via the load-cell of the test machine and the average through-thickness strain was recorded by a laser extensometer. The measured out-of-plane compressive response of the AL6XN pyramidal core is shown in Fig. 3. The core yields and then work hardens to a peak strength of $\sigma_p = 12.2$ MPa, associated with plastic buckling of the constituent struts [5]. A softening post-buckling response ensues, and finally struts begin to come into contact with the face-sheets and a hardening characteristic is observed.

The monotonic out-of-plane shear response of the core was measured by a single-lap shear test, as follows. A core containing 6.5 cells in the longitudinal direction (x_1) and three cells in the width direction (x_2) was brazed between type 304 stainless steel plates, giving a length to thickness ratio of $L/c = 12.7$; this satisfied the minimum required ratio of 12 as laid down by the ASTM standard C273-94 [16]. A sketch of the single-lap shear rig is shown in Fig. 4. Complementary shear implies that the shear loading in this test is identical to the shear loading that the core is subjected to in a three-point bend test. The out-of-plane shear stress on the core was measured via the load-cell of a screw-driven test machine, while the average through-thickness shear strain in the core was measured by a clip gauge attached to the face-sheets and straddling the core. The measured response has been added to Fig. 3 and displays a hardening response up to a peak strength of $\tau_p = 11.4$ MPa followed by fracture of the brazed joints.

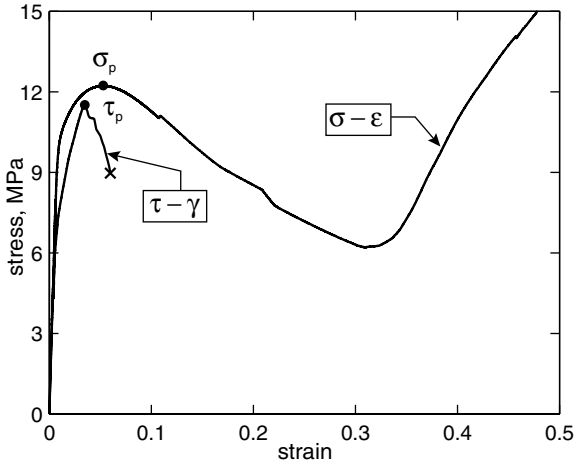

Fig. 3. The measured out-of-plane compressive response and longitudinal shear response of the $\bar{\rho} = 0.066$ AL6XN pyramidal core.

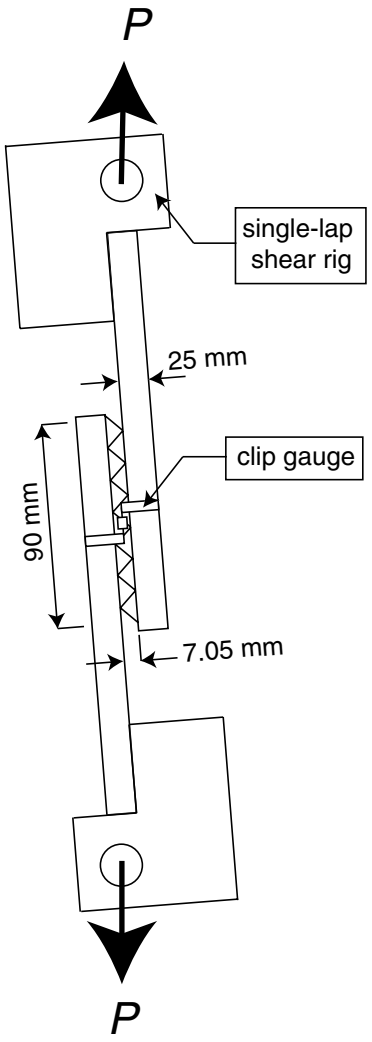

Fig. 4. Sketch of the single-lap shear test rig used for monotonic and cyclic tests.

2.3. Cyclic out-of-plane compressive response, and out-of-plane shear response of the AL6XN pyramidal core

Cyclic compression–compression tests were also performed on the sandwich specimens, using a servo-hydraulic test machine in load control at 20 Hz. Define the load ratio R as the ratio of minimum absolute load to maximum absolute load. A maximum load of 0.95 times the static collapse load was employed, with a load ratio $R = 0.1$ and 0.5. No fatigue failure was noted up to 10^7 cycles, and it is

concluded that the core is highly resistant to fatigue failure under out-of-plane compression–compression loading. In subsequent analysis it is assumed that the maximum absolute stress of the fatigue cycle at the endurance limit, σ_e, equals the peak compressive strength of the core in a monotonic test, σ_p.

Cyclic out-of-plane shear tests were conducted on the core using the same single-lap shear configuration as that used in the monotonic shear tests. The tests were performed at constant load range to specimen failure, and *S–N* fatigue curves were thereby obtained. All tests were performed at 20 Hz. The load ratio, defined by the ratio of minimum shear stress to maximum shear stress of the fatigue cycle was held at the values $R = 0.1$ and 0.5. The shear stress range is denoted $\Delta\tau$.

The shear strain at maximum load γ_{max} versus number of cycles N at selected stress ratios $\Delta\tau/\tau_p$ is shown in Fig. 5a and b for $R = 0.1$ and 0.5, respectively. The shear strain remains almost constant during an initial incubation period. Then, a sharp increase of γ_{max} occurs due to fatigue

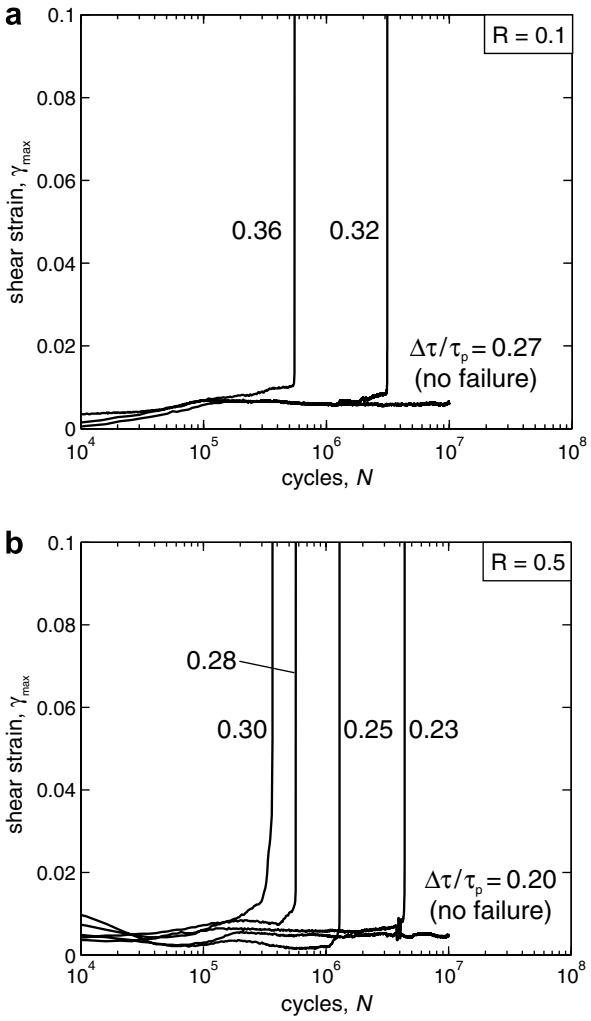

Fig. 5. The accumulated maximum shear strain γ_{max} versus number of cycles N at selected stress ranges $\Delta\tau/\tau_p$ and at load ratios (a) $R = 0.1$ and (b) $R = 0.5$.

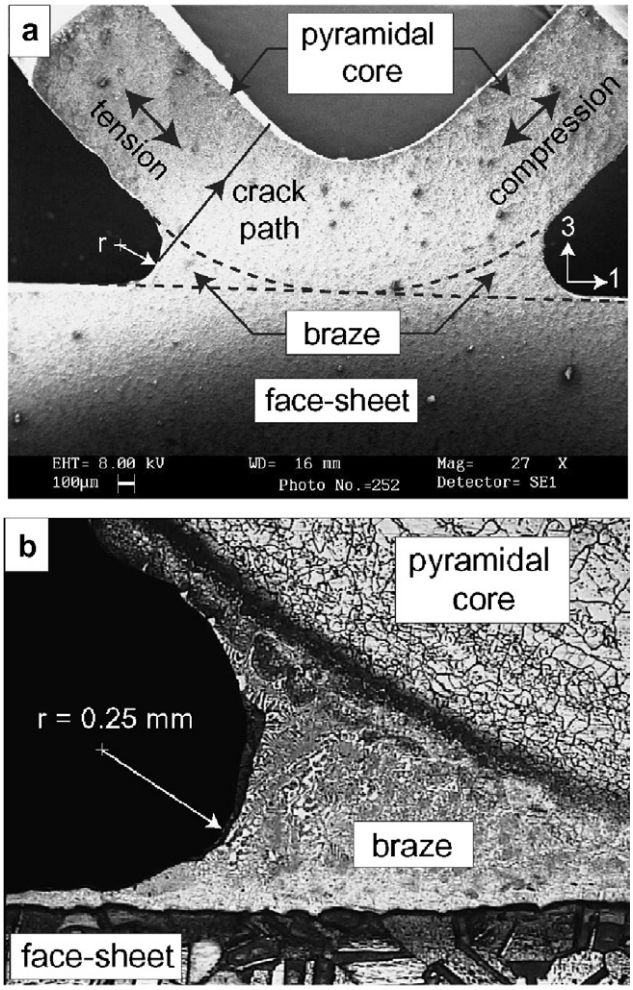

Fig. 6. (a) SEM photograph of a section of a undamaged joint showing the fatigue crack growth path starting at the toe of the braze joint of struts carrying tensile load. (b) Optical photograph of a polished braze joint showing the effect of diffusion bonding on the microstructure in the face-sheet and the pyramidal core. The radius arm of $r = 0.25$ mm forms a suitable scale bar for the image.

failure of a proportion of the struts within the core that carry tensile–tensile cyclic loads. Fatigue failure is defined by the number of cycles required for γ_{max} to attain an arbitrary but large value of 0.1. The fatigue life is insensitive to the precise level of γ_{max} beyond the knee of the curve, due to the steeply rising character of the curve.

Typically, fatigue cracks initiate at the interface between the brazed joint and the face-sheet, and propagate across the section of the strut. A representative scanning electron microscope (SEM) image of the joint detail and crack trajectory is given in Fig. 6a. In addition, an optical photograph of a polished and etched brazed joint is given in Fig. 6b.[1] Uniformly distributed phosphides are visible in the brazing joints similar to the observations in [17]. These

[1] The surface was prepared by successive grinding steps and a final polish with 1 µm diamond paste. The polished surface was then etched using a solution comprising 74% chloridric acid and 1.3% hydrogen peroxide.

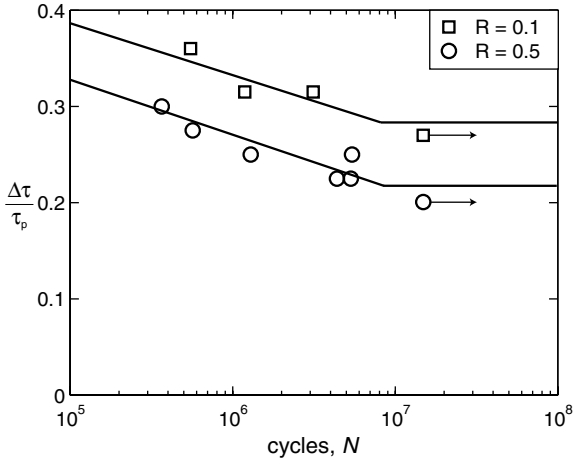

Fig. 7. *S–N* curves of pyramidal core in longitudinal shear loading for loading ratio $R = 0.1$ and 0.5.

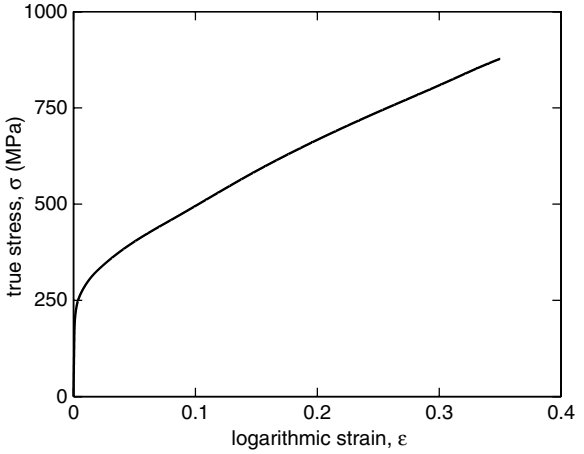

Fig. 8. The measured true tensile stress σ versus logarithmic strain ε response of 304 stainless steel in its brazed conditions. Measured Young's modulus $E = 210$ GPa and 0.1% offset yield strength of faces $\sigma_y = 210$ MPa.

phosphides decrease the ductility of the joint, and it is argued that they also degrade the fatigue strength.

The *S–N* curves are plotted in Fig. 7 and the measured shear endurance ratios at 10^7 cycles are $\Delta\tau_e/\tau_p = 0.27$ and 0.20 at $R = 0.1$ and 0.5, respectively. Thus, the endurance shear strength lies within the elastic range of the monotonic shear response (recall Fig. 3).

2.4. Monotonic and S–N fatigue response of the as-brazed AISI 304 stainless steel

The uniaxial tensile response of the AISI 304 stainless steel sheet was measured using a 1.2 mm thick dog-bone specimen of gauge length 50 mm and width 12.5 mm. Prior to testing, the specimen was subjected to the same braze cycle as that used to bond the core to 304 stainless steel faces: the dog-bone specimen was uniformly coated with the Ni–Cr 25-P10 (wt.%) brazing slurry, and was then placed in a vacuum furnace for 1 h at 1075 °C, using a dry argon atmosphere at 3–10 Pa.

The uniaxial tensile response was measured at a nominal strain rate of 10^{-4} s^{-1} using a screw-driven test machine; the axial load was measured from the load cell of the test machine, while the axial strain was measured via a laser extensometer. The measured true tensile stress σ versus logarithmic strain ε response of the AISI 304 stainless steel in the as-brazed condition is presented in Fig. 8. The measured Young's modulus and yield strength of this face-sheet material are $E = 210$ GPa and $\sigma_y = 210$ MPa, respectively.

Cyclic tension–tension tests were performed on the brazed AISI 304 stainless steel at constant load range in order to generate *S–N* curves to failure. The cyclic tests satisfied the ASTM standard E 466-82 [18], and were performed on 1.2 mm thick brazed dog-bone specimens, with a gauge length of 50 mm and width of 7.5 mm. The tests were conducted at 20 Hz using a servo-hydraulic machine, and the axial load was measured using the load-cell of the test machine.

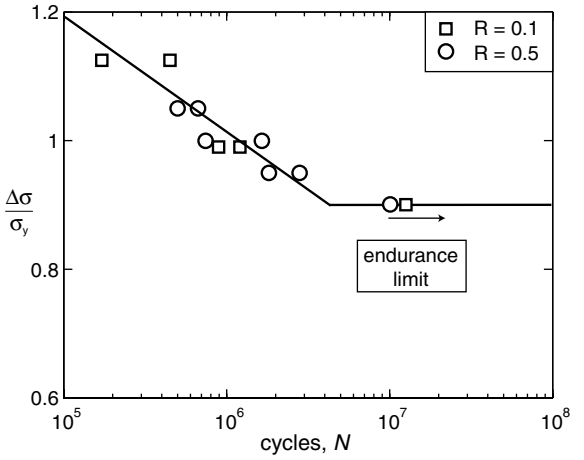

Fig. 9. The measured *S–N* curves for brazed 304 stainless steel under tension–tension cyclic loading for the load ratio $R = 0.1$ and 0.5.

Denote the minimum axial stress and maximum axial stress by σ_{min} and σ_{max}, respectively. Then the stress range is $\Delta\sigma = \sigma_{max} - \sigma_{min}$ and the *S–N* curves in the form of $\Delta\sigma$ versus number of cycles to failure are plotted in Fig. 9 for $R = \sigma_{min}/\sigma_{max} = 0.$ 1 and 0.5. An endurance ratio at 10^7 cycles of $\Delta\sigma_e/\sigma_y = 0.9$ is noted for both load ratios. It is worth noting that few cyclic tests with a pyramidal core brazed over the dog-bone specimen were performed in order probe the effect of the brazed joints on fatigue response. Similar endurance ratios were obtained indicating that imperfection introduced due to the brazing of the joints have a negligible effects on the measured fatigue response.

3. Failure mechanism map for monotonic loading of sandwich beams in three-point bending

Here we present analytical estimates and measurements of the three-point bend collapse response of sandwich

beams with a pyramidal core. While the analysis presented below relates specifically to three-point bending it can be generalised to the situation of a beam subjected to a shear force V and bending moment M as in Wicks and Hutchinson [19]. However, in this more general analysis, the indentation mode of collapse is neglected and hence we provide the more specialised analysis in this section.

3.1. Analytical formulae

Consider a sandwich beam in three-point bending made from rigid ideally-plastic materials. Upper bound formulae for the plastic collapse mechanisms have been derived by Ashby et al. [20] and these are employed to obtain a collapse mechanism map for monotonic loading. A photograph and a sketch of the three-point bending configuration are shown in Fig. 10.

3.1.1. Face yield

Face yield occurs at mid-span when the bending moment there attains the plastic collapse moment of the section. Neglecting contributions from plastic bending of the core, the critical load for face yield F_{FY} is given by

$$F_{\mathrm{FY}} = \frac{4bh(c+h)}{L}\sigma_{\mathrm{y}}, \tag{2}$$

where b is the width of the beam, h the face-sheet thickness, c the core thickness and L the sandwich beam span, as defined in Fig. 10. The yield strength of the face-sheet is denoted by σ_{y}.

3.1.2. Face wrinkling

The upper face-sheet is loaded in compression, and the maximum value of compressive stress is experienced directly beneath the central indenter. Face-sheet elastic wrinkling may occur when this axial stress attains a critical wrinkling stress σ_{w}. Now the pyramidal truss cores partitions the face-sheet into subsections of length l_1, which corresponds to the intercellular distance shown in Fig. 2. Euler elastic buckling of the face-sheet occurs at

$$\sigma_{\mathrm{w}} = \frac{k^2\pi^2 E}{12(1-\nu^2)}\left(\frac{h}{l_3}\right)^2, \tag{3}$$

where l_3 is the *reduced* intercellular distance taking in account the presence of brazing at the joint as shown in Fig. 2. The face-sheet Young's modulus is E. Since the width b is considerably greater than the thickness h, the subsections of the faces are considered as *wide columns* and hence the plane strain factor $1-\nu^2$ is introduced in the above equations. The factor k depends on the end-constraints set by the apex of the pyramidal. It is reasonable to assume that the faces are simply supported, giving $k=1$. Upon neglecting the contribution to the bending moment from the core, the collapse load for face wrinkling F_{FW} follows as

$$F_{\mathrm{FW}} = \frac{4bh(c+h)}{L}\sigma_{\mathrm{w}}. \tag{4}$$

3.1.3. Indentation

The indentation mechanism involves the formation of four plastic hinges within the top face-sheet adjacent to the central indenter, with compressive yield and shear of the underlying core. Rubino et al. [21] have performed an upper bound analysis taking into account both core compression and core shear. They find that the indentation load F_{I} is

$$F_{\mathrm{I}} = 2bh\sqrt{\sigma_{\mathrm{y}}\sigma_{\mathrm{p}}} + ab\sigma_{\mathrm{p}} + cb\tau_{\mathrm{p}}, \tag{5}$$

where a is the width of the indenter.

3.1.4. Core shear

The transverse shear load acting on a sandwich structure is carried mainly by the core. Failure by core shear mechanism occurs when the transverse shear stress reaches the shear strength of the pyramidal core. Depending upon the overhang length H of the sandwich beam (Fig. 10), two distinct core shear modes are possible, known as core shear mode A and core shear mode B (see [14] or [20] for details). The corresponding core shear collapse loads $F_{\mathrm{CS}}^{\mathrm{A}}$ and $F_{\mathrm{CS}}^{\mathrm{B}}$ are given by

$$F_{\mathrm{CS}}^{\mathrm{A}} = \frac{2bh^2}{L}\sigma_{\mathrm{y}} + 2bc\tau_{\mathrm{p}}\left(1+\frac{2H}{L}\right) \tag{6}$$

and

$$F_{\mathrm{CS}}^{\mathrm{B}} = \frac{4bh^2}{L}\sigma_{\mathrm{y}} + 2bc\tau_{\mathrm{p}}, \tag{7}$$

respectively.

For given geometrical parameters (L,H,h,a,b,c) and given material properties $(\sigma_{\mathrm{y}},\sigma_{\mathrm{p}},\tau_{\mathrm{p}})$, the operative collapse mechanism is associated with the lowest collapse load. A collapse mechanism map can be constructed with axes

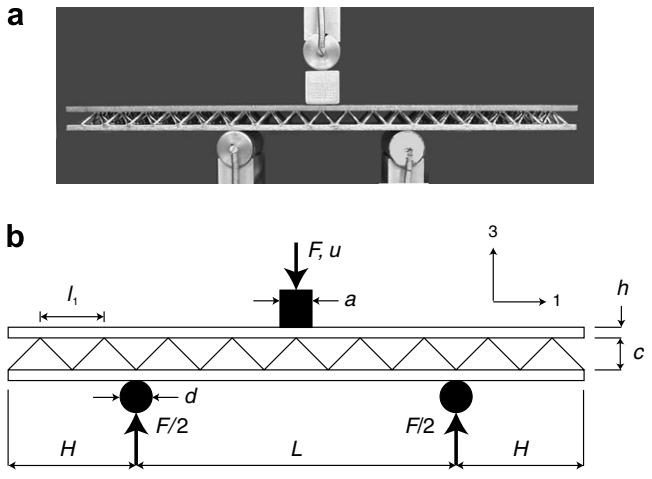

Fig. 10. (a) Photograph of a manufactured sandwich beam in three-point bending configuration with face-sheet thickness $h=2.95$ mm, span $L=90$ mm and core height $c=7.05$ mm (specimen S_1). (b) Sketch of pyramidal core sandwich beam showing the parameters involve in a three-point bending test.

h/c and c/L for selected σ_p/σ_y, τ_p/σ_y, H/L and a/L. One such collapse mechanisms map is plotted in Fig. 11, using the measured material properties and assuming $H/L = 1/4$ and $a/L = 1/16$. Five regimes are defined, denoting the anticipated dominant collapse mechanism: face yield, elastic face wrinkling, indentation, core shear mode A and core shear mode B. The indentation mode is not activated for any practical value of c/L due to the high compressive strength of the pyramidal core.

3.2. Experimental validation of the collapse mechanism map

Selected values of faces thickness h and span L were used in order to probe the competing collapse mechanisms in monotonic loading, as listed in Table 1. The sandwich beams were subjected to monotonic three-point bending to failure. The lower face of the sandwich beams was simply supported by rollers of diameter $d = 12.5$ mm and spacing L. The specimens were loaded at mid-span at a rate of 0.05 mm s^{-1} using a flat indenter of width $a = 14$ mm in order to avoid local indentation of the face. The applied load F was measured by the load-cell of the test machine, while the deflection u was measured by the LVDT gauge of the machine. The accuracy of the displacement measurements was validated by independent measurements with a laser displacement gauge. The pyramidal core possessed 19 cells in x_1-direction and four cells in the x_2-direction (Fig. 10), and was brazed between AISI 304 stainless steel faces of width 50 mm.

The specimen geometries and predicted failure modes have been added to the failure mechanism map shown in Fig. 11. The predicted collapse mode for most geometries is face yield, but for two geometries a different collapse mechanism is predicted: one for elastic face wrinkling and one for core shear B. The load versus displacement response for the specimen collapsing by face wrinkling and for the specimen failing by face yield are given in Figs. 12 and 13, respectively. A representative collapse response for one of the specimens failing by core shear B is given in Fig. 14. A photograph of the collapsed specimen is shown in each of Figs. 12–14. A comparison of the measured collapse load F_{exp} and predicted load F_{pred} are listed in Table 1. For core shear and elastic face wrinkling failure, F_{exp} is set by the measured peak load. No load peak was observed in the face yielding mode and so the plastic collapse was to define F_{exp}, see Fig. 13b. The observed collapse mechanism and measured collapse load were in broad agreement with the predictions, see Table 1.

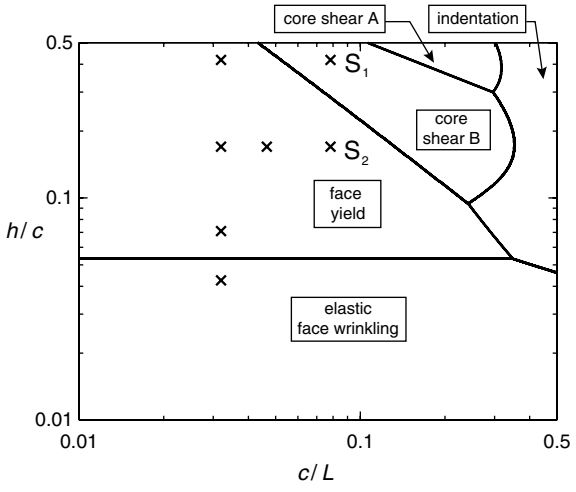

Fig. 11. Failure mechanisms map with h/c and c/L as axes for a sandwich beam with AL6XN pyramidal core of relative density $\bar{\rho} = 0.066$, using the measured material properties and beam geometries $H/L = 1/4$ and $a/L = 1/16$. The data points denote the tested geometries in monotonic loading. The specimens S_1 and S_2 are also explored in fatigue.

4. Fatigue mechanism map for cyclic loading of sandwich beams in three-point bending

The fatigue strength of the faces and core governs the fatigue properties of the sandwich structure. It is instructive to construct a fatigue mechanism map in order to show the dependence of fatigue failure mechanism upon sandwich beam geometry. The collapse strength formulae given above are now modified to account for cyclic loading. Expressions are obtained for the endurance limit for each fatigue mechanism.

4.1. Analytical formulae

Consider first *face fatigue*. The endurance load range for face fatigue ΔF_{FY} is obtained by replacing the yield strength of the face-sheet σ_y in (2) with the endurance range $\Delta\sigma_e$ to give

$$\Delta F_{FY} = \frac{4bh(c+h)}{L}\Delta\sigma_e. \tag{8}$$

Face wrinkling in fatigue is by the same mechanism of elastic wrinkling as given by the formula (3) for monotonic loading. Hence, the stress range in the face $\Delta\sigma_w$ is related to the elastic wrinkling stress σ_w by $\Delta\sigma_w = (1 - R)\sigma_w$, and the expression (4) provides the load range for face wrinkling ΔF_{FW} as

$$\Delta F_{FW} = (1 - R)F_{FW}. \tag{9}$$

Now consider *indentation under cyclic loading*, and write ΔF_I as the load range for indentation at the endurance limit. Recall that the pyramidal core is immune to compression–compression fatigue while there is a considerable knockdown in the shear strength under cyclic loading. Thus, the maximum indentation load under cyclic loading is given by

$$F_{I\max} = 2bh\sqrt{\frac{\Delta\sigma_e}{1-R}\sigma_p} + ab\sigma_p + cb\frac{\Delta\tau_e}{1-R}. \tag{10}$$

The cyclic indentation strength follows as

$$\Delta F_I = 2bh\sqrt{(1-R)\Delta\sigma_e\sigma_p} + ab\sigma_p(1-R) + cb\Delta\tau_e. \tag{11}$$

Table 1
Details of specimen tested monotonically in three-point bending

Specimen designation	h (mm)	L (mm)	Predicted and observed collapse mode	F_{pred} (kN)	F_{exp} (kN)	Error (%)
1	0.3	220.5	Elastic face wrinkling	0.31	0.36	−16.1
2	0.5	220.5	Face yielding	0.72	0.63	+12.5
S_2, 3	1.2	90.0	Face yielding	4.62	4.93	−6.7
4	1.2	151.5	Face yielding	2.76	2.75	+0.1
5	1.2	220.5	Face yielding	1.89	1.85	+2.1
6	2.95	220.5	Face yielding	5.63	5.30	+5.9
S_1, 7	2.95	90.0	Core shear B	11.95	11.50	+3.8

The two specimen geometries tested under cyclic loading are marked S_1 and S_2.

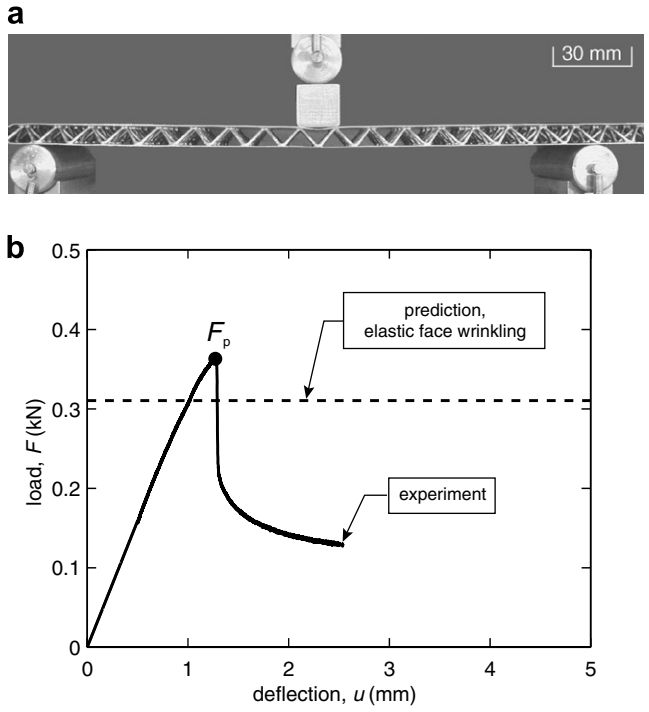

Fig. 12. (a) Photograph of a monotonically loaded deformed specimen with $h = 0.3$ mm and $L = 220$ mm. It collapses by elastic face wrinkling. (b) The F versus u response for this specimen along with the analytical prediction of the collapse strength.

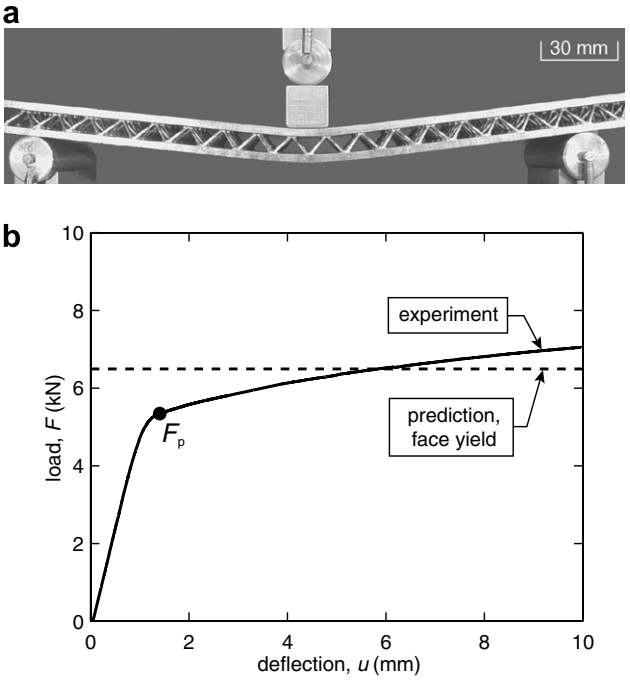

Fig. 13. (a) Photograph of a monotonically loaded deformed specimen with $h = 2.95$ mm and $L = 220$ mm. It collapses by face yielding. (b) The F versus u response for this specimen along with the analytical prediction of the collapse strength.

Finally, consider fatigue failure of the sandwich beam by *core shear*. Recall from the S–N curves of Fig. 7 that the endurance strengths at 10^7 cycles are $\Delta\tau_e/\tau_p = 0.27$ and 0.2 for $R = 0.1$ and 0.5, respectively. These stress levels fall within the elastic range of the core, and so the upper bound expressions (Eqs. (6) and (7)) for plastic collapse by core shear are unsuitable for cyclic loading. Instead, it is assumed that under cyclic loading the shear stress distribution across a section of the sandwich beam is given by the elastic solution. The contribution to the bending moment from the pyramidal core is negligible, and it can be assumed that the shear stress does not vary across the core portion of the beam cross-section [13,22]. A strength of materials calculation relates the cyclic shear stress within the core $\Delta\tau_e$ at the endurance limit to the applied load range ΔF_{CS}:

$$\Delta F_{CS} = \frac{2h^2/3 + 2(c+h)^2}{c+h} b\Delta\tau_e. \tag{12}$$

The formulae (8)–(12) allow for the construction of a fatigue mechanism map with axes h/c and c/L. The operative collapse mechanism is associated with the lowest load range ΔF. Such a map is shown in Fig. 15 for $R = 0.1$ and $R = 0.5$, upon assuming the measured values of fatigue strength for faces and core, and taking $H/L = 1/4$ and $a/L = 1/16$. We note that the fatigue failure regime of core shear expands with increasing R due to the decreased cyclic shear strength of the core with increasing R.

4.2. Critical experiments to validate the map

Two designs were considered in the fatigue tests, labelled S_1 and S_2 on the map of Fig. 15. The span was fixed at $L = 90$ mm and the face thickness was 2.95 mm for specimen S_1 and 1.2 mm for specimen S_2. These values were chosen such that specimen S_1 failed by core shear in both the monotonic and cyclic tests; in contrast, specimen S_2

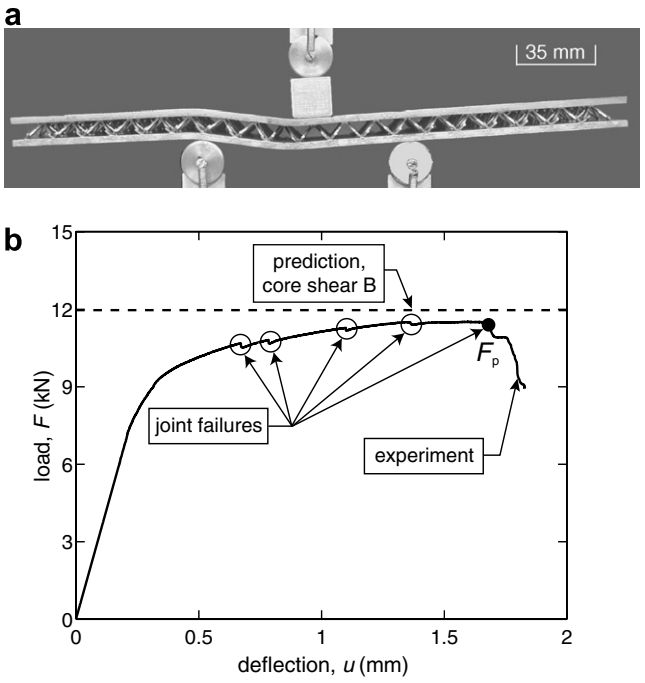

Fig. 14. (a) Photograph of a monotonically loaded deformed specimen S_1 with $h = 2.95$ mm and $L = 90$ mm. It collapses by core shear B. (b) The F versus u response for this specimen along with the analytical prediction of the collapse strength.

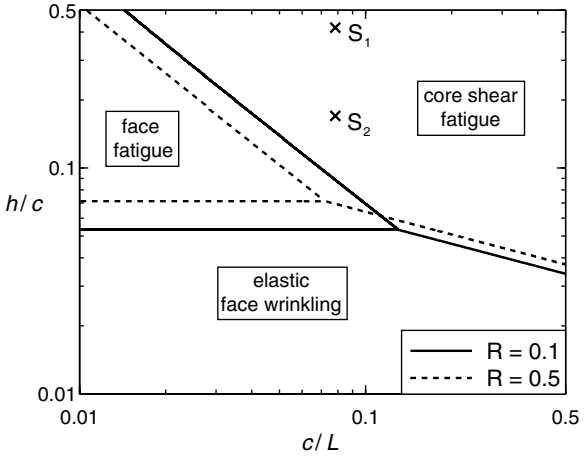

Fig. 15. The fatigue failure mechanisms map with h/c and c/L as axes for a sandwich beam with AL6XN pyramidal core of relative density $\bar{\rho} = 0.066$, using the measured material properties and beam geometries $H/L = 1/4$ and $a/L = 1/16$ The specimens S_1 and S_2 denote the tested geometries in cyclic loading. Maps are shown for two different loading ratios: $R = 0.1$ and $R = 0.5$.

failed by core shear fatigue in the cyclic tests and by face yield in the monotonic test.

Sandwich beams were subjected to cyclic three-point bending to failure using a servo-hydraulic test machine in load control at 20 Hz. The applied load F was measured by the load-cell of the test machine whilst the deflection u was measured by the LVDT gauge of the machine. Both geometries of sandwich beam were tested at the load ratio $R = F_{min}/F_{max}$ of 0.1 and 0.5, and at selected values of the load range $\Delta F = F_{max} - F_{min}$.

The maximum deflection u_{max} versus number of cycles N at selected load levels $\Delta F/F_p$ of the design S_1 is shown in Fig. 16 for both R values, where F_p is the measured monotonic collapse load. In similar manner to that described in Section 2.3 for single-lap shear of the core, fatigue failure occurs at the brazed joints. A SEM image of the failed section of a strut is shown in Fig. 17, confirming the crack trajectory.

As predicted, specimen S_1 failed by core fatigue in the cyclic tests and by core shear under monotonic loading. The S–N curve for the sandwich beam S_1 is plotted in Fig. 18, along with best-fitting S–N curves for cyclic shear of the core (transcribed from Fig. 7). The measurements overlap as expected from the simple micromechanical models of cyclic failure given by Eq. (12). Now consider the sandwich beam specimen S_2. This geometry failed by face yield under monotonic loading and by core shear under fatigue loading, as suggested by the maps of Figs. 11 and 15. The S–N curve for this sandwich beam is plotted in Fig. 18, with ΔF normalised by the measured collapse strength F_p associated with the *different*

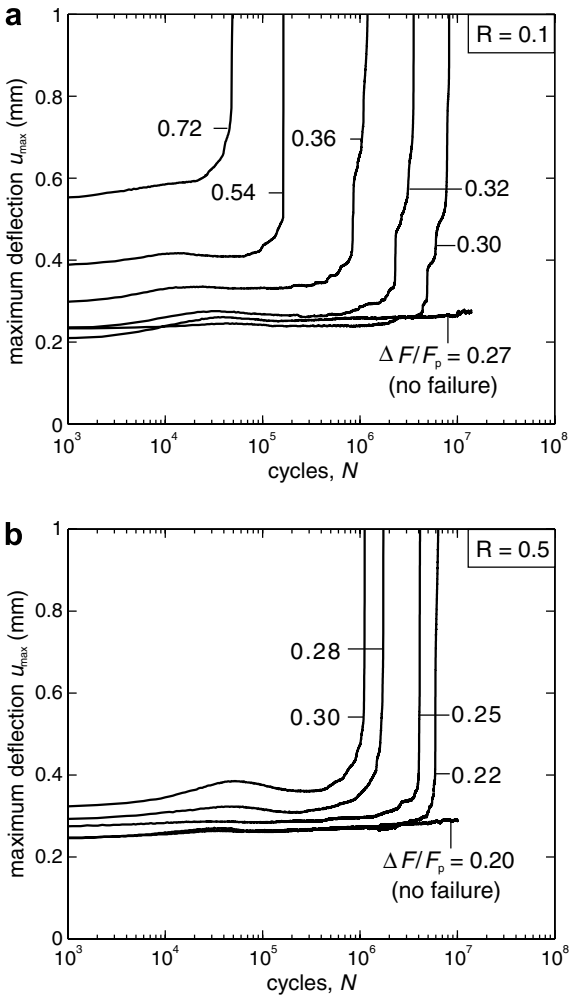

Fig. 16. The maximum deflection u_{max} versus number of cycles N of sandwich beam S_1 ($h = 2.95$ mm and $L = 90$ mm) at selected loading levels $\Delta F/F_p$ for load ratios: (a) $R = 0.1$ and (b) $R = 0.5$.

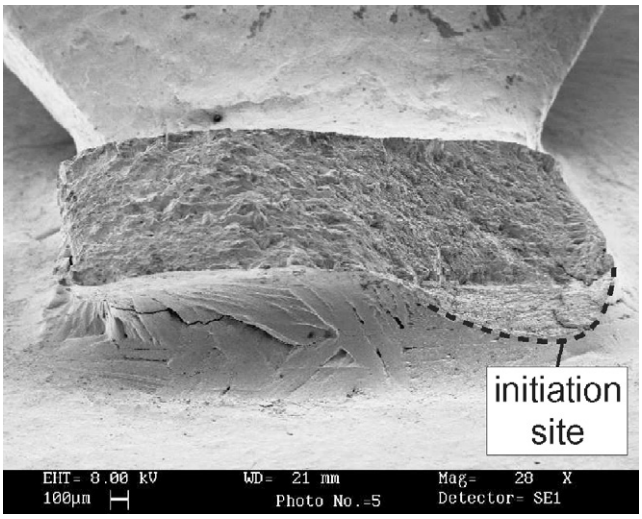

Fig. 17. SEM photograph of fracture surface clearly showing fatigue crack initiation at the toe of the brazed joint.

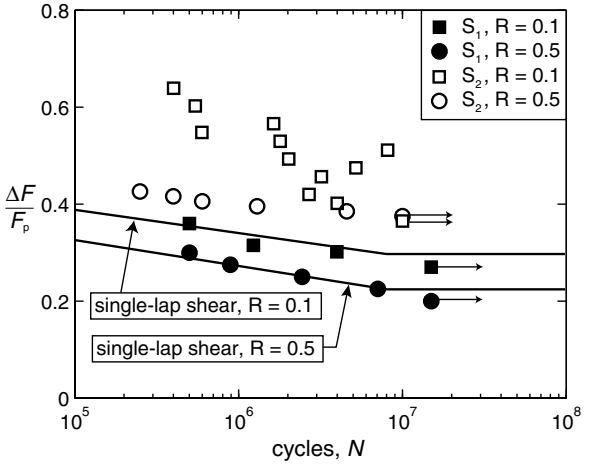

Fig. 18. Fatigue S–N curves of load range ΔF normalised by the peak load F_p for sandwich beams S_1 and S_2. Data for load ratios $R = 0.1$ and 0.5 are included. Single-lap shear S–N curves for the pyramidal core have been transcribed from Fig. 7 for comparison purposes.

mechanism (i.e. face yield). Consequently, the data does not overlap the S–N curves for cyclic shear of the core (transcribed from Fig. 7). However, the endurance strength as predicted by Eq. (11) for specimen S_2 is in good agreement with the measured value for $R = 0.5$ and is about 30% higher for $R = 0.1$.

5. Concluding remarks

In this study, competing mechanisms of monotonic and cyclic failure are compared for sandwich beams with a pyramidal lattice core made from AL6XN stainless steel. This steel is of interest for marine applications due to its extreme corrosion resistance. It is found that the presence of the brazed joints leads to a significant knock-down in the shear strength of the core under cyclic loading, but to no drop in strength under compression–compression fatigue. This knock-down in strength should be included in design calculations for sandwich structures employing the pyramidal lattice core with brazed joints.

Simple micromechanical models are used to estimate both the monotonic collapse load and the fatigue strength of sandwich beam with the lattice core. These models have adequate predictive capability and are useful for constructing monotonic and cyclic failure maps. Typical maps have been generated in this study and have been validated by selected measurements of sandwich beam strength under monotonic and cyclic loading.

Acknowledgements

The authors are grateful to ONR for their financial support through US-ONR IFO grant number N00014-03-1-0283 on The Science and Design of Blast Resistant Sandwich Structures. FC acknowledges support from the Cambridge Commonwealth Trust and the Fonds québécois de la recherche sur la nature et les technologies.

References

[1] Gibson LJ, Ashby MF. Cellular solids, structure and properties. second ed. Cambridge: Cambridge University Press; 1997.
[2] Deshpande VS, Fleck NA, Ashby MF. Effective properties of the octet–truss lattice material. J Mech Phys Solids 2001;49(8):1747–69.
[3] Ashby MF. Multi-objective optimization in material design and selection. Acta Mater 2000;48(1):359–69.
[4] Evans AG, Hutchinson JW, Fleck NA, Ashby MF, Wadley HNG. The topological design of multifunctional cellular metals. Progr Mater Sci 2001;46:309–27.
[5] Zok FW, Waltner SA, Wei Z, Rathbun HJ, McMeeking RM, Evans AG. A protocol for characterizing the structural performance of metallic sandwich panels: application to pyramidal truss cores. Int J Solids Struct 2004;41(22-23):6249–71.
[6] Harte A-M, Fleck NA, Ashby MF. Fatigue failure of an open cell and a closed cell aluminium alloy foam. Acta Mater 1999;47(8):2511–24.
[7] Sugimura Y, Rabiei A, Evans AG, Harte A-M, Fleck NA. Compression fatigue of a cellular Al alloy. Mater Sci Eng A 1999;269(1–2):38–48.
[8] Fleck NA, Kang KJ, Ashby MF. Overview No. 112: the cyclic properties of engineering materials. Acta Metall Mater 1994;42(2):365–81.
[9] McCullough KYG, Fleck NA, Ashby MF. The stress-life behaviour of aluminium alloy foams. Fatigue Fract Eng Mater Struct 2000;23:199–208.
[10] Harte A-M, Fleck NA, Ashby MF. The fatigue strength of sandwich beams with an aluminium alloy foam core. Int J Fatigue 2001;23(6):499–507.
[11] Burman M, Zenkert D. Fatigue of foam core sandwich beams—1: undamaged specimens. Int J Fatigue 1997;19(7):551–61.
[12] Werren F. Shear-fatigue properties of various sandwich constructions. US Forest Prod Lab Report 1837, 1952.
[13] Zenkert D. An introduction to sandwich construction. London: Emas Publishing; 1995.
[14] Deshpande VS, Fleck NA. Collapse of truss core sandwich beams in 3-point bending. Int J Solids Struct 2001;38:6275–305.
[15] Wadley HNG, Fleck NA, Evans AG. Fabrication and structural performance of periodic metal sandwich structures. Comp Sci Tech 2003;63:2331–43.

[16] ASTM Standard C273-94. Standard test method for shear properties of sandwich core materials. American Society for Testing and Materials; 1994.
[17] Zhuang WD, Eagar TW. Transient liquid-phase bonding using coated metal powders. Welding J 1997;76(4):157–162s.
[18] ASTM Standard E466-82. Standard practice for conducting constant amplitude axial fatigue tests of metallic material. American Society for Testing and Materials; 1982.
[19] Wicks N, Hutchinson JW. Performance of sandwich plates with truss cores. Mech Mater 2004;36:739–51.
[20] Ashby MF, Evans AG, Fleck NA, Gibson LJ, Hutchinson JW, Wadley HNG. Metal foams: a design guide. Oxford: Butterworth Heinemann; 2000.
[21] Rubino V, Deshpande VS, Fleck NA. The collapse response of sandwich beams with a Y-frame core subjected to distributed and local loading. Int J Mech Sci, 2007 (submitted for publication).
[22] Allen HG. Analysis and design of structural sandwich panels. Oxford: Pergamon Press; 1969.